Palaeogeography, Palaeoclimatology, Palaeoecology 493 (2018) 44–54

Contents lists available at ScienceDirect

Palaeogeography, Palaeoclimatology, Palaeoecology

journal homepage: www.elsevier.com/locate/palaeo

Hydrological variability in the western tropical Pacific over the past 700 kyr and its linkage to Northern Hemisphere climatic change

Qi Jia[a,c], Tiegang Li[b,c,d,*], Zhifang Xiong[b,d,*], Stephan Steinke[e], Fuqing Jiang[a,d], Fengming Chang[a,d], Bingbin Qin[b]

[a] Key Laboratory of Marine Geology and Environment, Institute of Oceanology, Chinese Academy of Sciences, Qingdao 266071, China
[b] First Institute of Oceanography, State Oceanic Administration, Qingdao 266061, China
[c] University of Chinese Academy of Sciences, Beijing 100049, China
[d] Laboratory for Marine Geology, Qingdao National Laboratory for Marine Science and Technology, Qingdao 266061, China
[e] Department of Geological Oceanography, College of Ocean and Earth Sciences, Xiamen University, Xiamen 361102, China

ARTICLE INFO

Keywords:
Western Philippine Sea
Seawater $\delta^{18}O$ estimates
Sea surface temperature
ENSO
ITCZ
AMOC

ABSTRACT

El Niño/Southern Oscillation (ENSO) events and latitudinal shifts of the Intertropical Convergence Zone (ITCZ) cause large scale hydrologic changes in the western tropical Pacific (WTP). However, there is still a debate on the role of ENSO and ITCZ shifts on the hydroclimate in the WTP and their linkage to Northern Hemisphere climate change on glacial-interglacial timescales. For that reason, we present ice volume-corrected seawater $\delta^{18}O$ ($\delta^{18}O_{sw\text{-}ice}$, a proxy for salinity) and sea surface temperature (SST) records from IMAGES Core MD06-3047B recovered from the northern WTP to investigate the hydroclimate in the WTP during the last 700 kyr. Planktic foraminifera *Globigerinoides ruber* based Mg/Ca-SST and $\delta^{18}O_{sw\text{-}ice}$ records reveal distinct glacial-interglacial variations. The $\delta^{18}O_{sw\text{-}ice}$ record shows that our study site is characterized by fresher conditions and thus higher precipitation during glacials than during interglacials. Our results are in good agreement with numerical model simulations, which also suggest a glacial freshening in the northern WTP. A glacial freshening of the WTP is most likely related to a substantial weakening of the Atlantic Meridional Overturning Circulation (AMOC) and/or exposure of the Maritime Continent due to sea level changes which resulted in an enhanced Pacific Walker circulation and/or southward shift of the ITCZ. In addition, SST records from the WTP and the eastern tropical Pacific (ETP) suggest an enhanced tropical Pacific zonal SST gradient and thus La Niña-like conditions, which may have contributed to fresher conditions in the WTP during glacial periods. Besides, our rainfall record is in antiphase to the Chinese speleothem $\delta^{18}O$ records, supporting the idea of an opposing trend in precipitation changes between the WTP and East Asia on orbital timescales.

1. Introduction

The Western Pacific Warm Pool (WPWP) is characterized by annual sea surface temperature (SST) above 28 °C and is the world's largest center of tropical convection. It was therefore suggested that the WPWP plays an important role in global climate change (Cane, 1998; Hoerling et al., 2001; Yan et al., 1992). The spatial and temporal evolution of the WPWP is closely linked to large-scale climatic features, such as the El Niño/Southern Oscillation (ENSO) and latitudinal shifts in the mean position of the Intertropical Convergence Zone (ITCZ). In modern climate, ENSO and shifts of the ITCZ control precipitation and sea surface salinity (SSS) in the western tropical Pacific (WTP) (Delcroix et al., 1996; Ropelewski and Halpert, 1987; Schneider et al., 2014). ENSO and related changes in the strength and position of the Walker circulation also affect zonal hydrologic characteristics over the tropical Pacific (Delcroix et al., 1996; Deser and Wallace, 1990; Trenberth and Caron, 2000). During El Niño years, a breakdown of the Walker circulation results in a net reduction in precipitation over the WTP (Lyon et al., 2006; Ropelewski and Halpert, 1987). The opposite occurs during La Niña years.

The importance of the WPWP is best manifested by ENSO, which affects climate globally (Cane, 1998; Halpert and Ropelewski, 1992; Ropelewski and Halpert, 1987). For that reason, many studies investigated ENSO activity (e.g. Carre et al., 2014; Ford et al., 2015; Koutavas and Joanides, 2012; Leduc et al., 2009a; Liu et al., 2014; Otto-Bliesner et al., 2003; Tudhope et al., 2001; Zhang et al., 2014; Zheng et al., 2008) and ENSO-like state (e.g. Lea et al., 2000; Martínez et al., 2003; Stott et al., 2002) on different timescales. Planktic foraminiferal

* Corresponding authors at: First Institute of Oceanography, State Oceanic Administration, Qingdao 266061, China.
E-mail addresses: tgli@fio.org.cn (T. Li), zhfxiong@fio.org.cn (Z. Xiong).

https://doi.org/10.1016/j.palaeo.2017.12.039
Received 26 September 2017; Received in revised form 23 December 2017; Accepted 30 December 2017
Available online 05 January 2018
0031-0182/ © 2018 Elsevier B.V. All rights reserved.

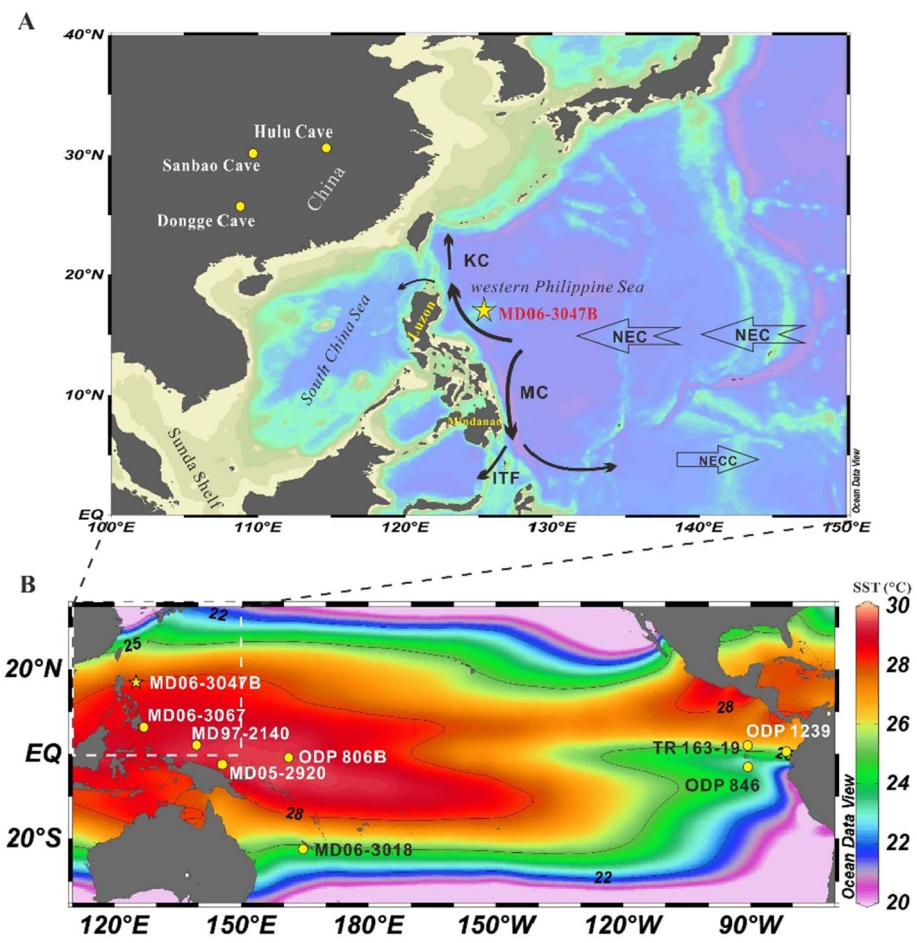

Fig. 1. Location of Core MD06-3047B (yellow star). A: bathymetric map showing the surface currents in the northern part of western Pacific. Ocean currents are according to Fine et al. (1994). NEC: North Equatorial Current, NECC: North Equatorial Counter Current, KC: Kuroshio Current, MC: Mindanao Current, and ITF: Indonesian Throughflow. Yellow dots indicate Sanbao, Dongge and Hulu Caves. B: sediment cores also discussed in this study are indicated by yellow dots. SST in B are annual mean SST from World Ocean Atlas 2013 (Locarnini et al., 2013). (For interpretation of the references to colour in this figure legend, the reader is referred to the web version of this article.)

oxygen isotopic ratios and SST records from deep-sea sediments show a reduced tropical Pacific zonal temperature gradient during Last Glacial Maximum (LGM), which was interpreted to reflect more El Niño-like conditions with an increase in El Niño events (Koutavas et al., 2002) or amplified ENSO state (Koutavas and Joanides, 2012). El Niño-like conditions during the last glacial period were also deduced from salinity records of a sediment core near the coast of Mindanao (Stott et al., 2002). However, Martínez et al. (2003) suggested that La Niña-like conditions prevailed in the eastern equatorial Pacific during the last glaciation. In addition, SST records spanning several glacial-interglacial cycles also revealed a larger zonal SST gradient and north-south SST gradient across the eastern tropical Pacific (ETP) during glacials, indicating La Niña-like conditions (Lea et al., 2000; Rincón-Martínez et al., 2010; Zhang et al., 2016). In summary, contrasting findings exist about the background state of the tropical Pacific: the studies of Beaufort et al. (2001), Jiang et al. (2016), Lea et al. (2000), Martínez et al. (2003), and Rincón-Martínez et al. (2010) proposed La Niña-like conditions during glacial periods, whereas several other studies suggested El Niño-like conditions during glacial periods (Koutavas and Joanides, 2012; Sagawa et al., 2012; Koutavas et al., 2002; Stott et al., 2002). It was also proposed that north-south shifts of the ITCZ in response to changes in the interhemispheric temperature gradient exert a major influence on the precipitation patterns and monsoon dynamics (Deplazes et al., 2013; Fleitmann et al., 2007; Schmidt and Spero, 2011). The northward migration of the ITCZ results in high precipitation over the northern regions of the WTP, while the reverse occurs during southward shift of the ITCZ (Schneider et al., 2014). The precipitation changes are accompanied by changes in SSS (Delcroix et al., 1996). Leduc et al. (2009b) and Schmidt and Spero (2011) suggested that the migration of the ITCZ is the main driver of precipitation changes in the tropics/subtropics on different timescales.

Shifts in the mean climate state in the tropical Pacific were proposed to be mainly related to climatic changes in the high latitudes (DiNezio and Tierney, 2013; Schmidt and Spero, 2011; Xiang et al., 2009; Zhang and Delworth, 2005). Numerical model simulations by Zhang and Delworth (2005) suggested that a substantial weakening of the Atlantic Meridional Overturning Circulation (AMOC) causes significant atmospheric circulation changes over the tropical Pacific. In addition, model simulation and proxy results showed that the WTP experienced significant hydrologic changes during the LGM due to variations in the Pacific Walker circulation caused by exposure of the Maritime Continent due to sea level changes (DiNezio et al., 2011; DiNezio and Tierney, 2013). Climate simulations also indicated that changes in interhemispheric temperature asymmetry cause north/south ITCZ shifts on glacial-interglacial timescales (Broccoli et al., 2006). Model results and paleoclimate data both suggested that the southward displacement of the ITCZ during glacials may be forced by cooler conditions or increased ice sheets in the Northern Hemisphere (Broccoli et al., 2006; Chiang and Bitz, 2005; Schneider et al., 2014).

Various long-term planktic foraminiferal SST and stable oxygen isotopes ($\delta^{18}O_{calcite}$) records have been obtained from different parts of the tropical Pacific, which make it possible to reconstruct the spatial characteristics of precipitation changes over the WTP. However, long-term records of changes in SST and SSS records in the northern WTP are still missing. Here, we present new *Globigerinoides ruber* (*G. ruber*) Mg/Ca-based SST and stable oxygen isotope reconstructions from a sediment core retrieved from the northern WTP. The combination of Mg/Ca measurements and stable oxygen isotopes of the planktic foraminifera *G. ruber* allows us to investigate the hydrographic history of the northern WTP over the last 700 kyr and to discuss its forcing

mechanisms. In addition, by integrating previously published SST records from other sites in the tropical Pacific with our new SST records from the northern WTP, we assess variations in the tropical Pacific zonal SST gradient during the last 700 kyr.

2. Study area—oceanography and climate

The Northern Equatorial Current (NEC) and the Kuroshio Current (KC) are the main surface currents in the western Philippine Sea (Fig. 1A). After reaching the coast of the Philippines, the NEC splits into two branches at ~15°N (Toole et al., 1990). The northward branch contributes to the KC, whereas the southward branch forms the Mindanao Current (MC), which ultimately contributes to the Indonesian Throughflow (ITF). The average modern annual SST near our study area is ~28.1 °C (Locarnini et al., 2013).

The climate regime over the western Philippine Sea and nearby Philippines is dominated by the East Asian monsoon. Rainfall is highest during the summer monsoon season between May and October. During the winter monsoon season, dry winds from the northeast prevail from November through April. The latitudinal shifts of the ITCZ and related monsoon variations cause seasonal precipitation and SSS changes in our study area, with higher precipitation and lower SSS during the northward shift of the ITCZ (Figs. 2A and B; S1and S2). On the other hand, observational data indicate that ENSO can also exert a strong influence on the rainfall patterns and thus SSS in our study area. During La Niña (El Niño) years, the study area is characterized by higher (lower) SST with enhanced (decreased) precipitation and relative low (high) SSS (Figs. 2C and D; S1 and S2).

3. Materials and methods

3.1. Sediment core MD06-3047B

Core MD06-3047B (17° 00.44′ N, 124° 47.93′ E) was retrieved from the Benham Rise in the western Philippine Sea during the R/V Marion Dufresne/IMAGES XIV cruise in 2006 (Fig. 1A). The core location is about 240 km east off Luzon and Core MD06-3047B was retrieved from a water depth of 2510 m. The core length is 8.90 m. The Benham Rise is a plateau which was formed at about 50–45 Ma (Hilde and Lee, 1984). The core mainly consists of yellowish-brown silty clay without any evidence of turbidities or mass wasting deposits. The modern location of Core MD06-3047B is well above the modern lysocline (~3400 m) where carbonate preservation is expected to be good (Berger et al., 1982; Groetsch et al., 1991). Pteropod shells were also found in our samples, which further indicates a good carbonate preservation.

3.2. Oxygen isotope analyses

The benthic foraminifera *Fontbotia wuellerstorfi* (also commonly referred to as *Cibicidoides* or *Planulina wuellerstorfi*) and the surface-dwelling planktic foraminifera *Globigerinoides ruber* (white) were selected from samples at 2 cm and 4 cm intervals for isotopic analysis. The *F. wuellerstorfi* (around 5–8 individuals) and *G. ruber* (around 25–30 individuals) were picked from the 300–355 μm and 250–300 μm size fraction, respectively. The foraminiferal shells were crushed into several fragments, soaked in 3–5% hydrogen peroxide to remove organic material, washed with acetone in an ultrasonic bath for 30 s, rinsed three times with water, and dried at 50 °C. Stable oxygen isotope ratios of the benthic and planktic foraminiferal tests were measured on a GV IsoPrime mass spectrometer at the Key Laboratory of Marine Geology and Environment, Institute of Oceanography, Chinese Academy of Sciences, Qingdao. Values are reported relative to the Pee Dee

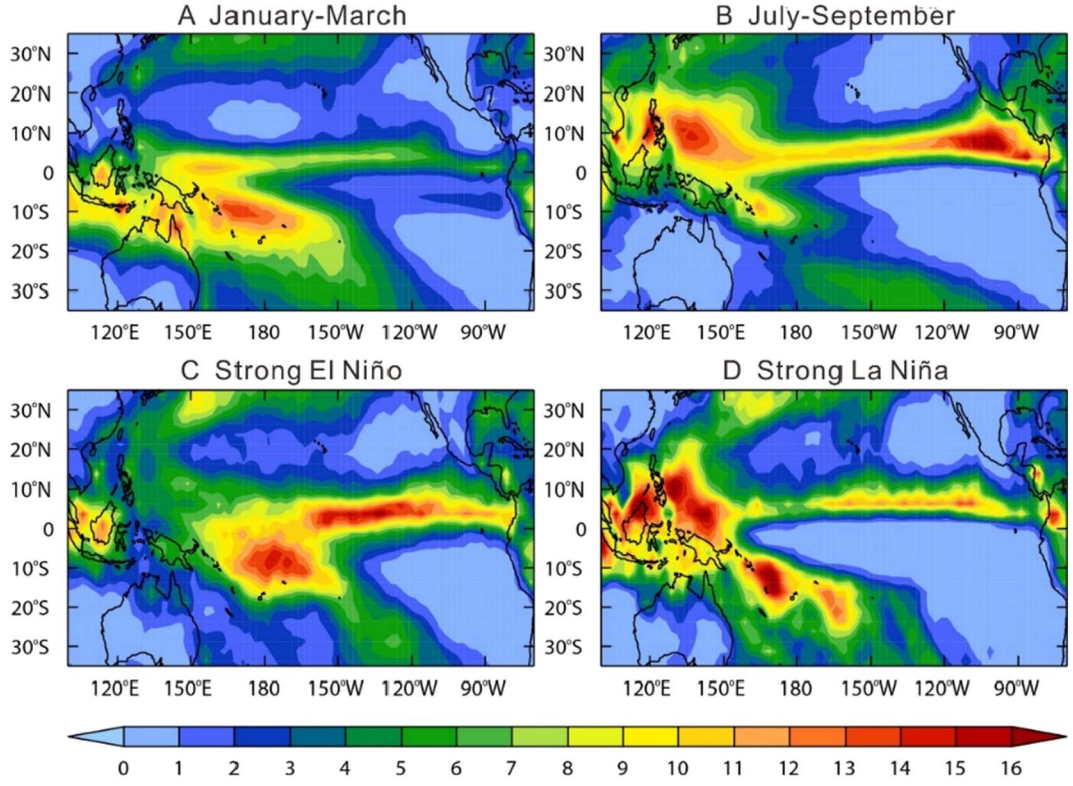

Fig. 2. Tropical Pacific mean precipitation rates (in mm day^{-1}) derived from the Climate Prediction Center Merged Analysis of Precipitation (CMAP) standard, for the time interval 1979–2016 averaged, A and B: for January to March and for July to September, C and D: for December to February during strong El Niño years and during strong La Niña years. The precipitation data are available at https://www.esrl.noaa.gov/psd/data/gridded/data.cmap.html, the ENSO information are from http://ggweather.com/enso/oni.htm.

Belemnite (PDB), calibrated by using the National Bureau of Standards (NBS) 18. The long-term reproducibility for stable oxygen isotope measurements which is based on replicate measurements of a reference standard UCD-SM92 ($\delta^{18}O = -1.94‰$), is ± 0.06‰ (1σ).

3.3. Mg/Ca analyses and SST estimates

For Mg/Ca analysis, *G. ruber* was selected from samples at 4-cm intervals and around 50–60 individuals were picked from the 250–300 μm size fraction and from the 200–250 μm size fraction, when *G. ruber* individuals were not sufficient from the fraction 250–300 μm. The planktonic tests were pretreated and cleaned following the cleaning method of Boyle and Keigwin (1985/1986) and Martin and Lea (2002). The cleaning procedure included three water rinses, two methanol rinses, and two additional water rinses to remove any loosely-adhering contaminations, such as clays. Thereafter, a hot basic reducing treatment using a hot, buffered solution of hydrous hydrazine was used to reduce and solubilize iron and manganese oxides likely precipitated on the surface of the planktic foraminiferal tests. An oxidizing solution in a hot, alkali-buffered solution of H_2O_2 was used to oxidize and solubilize organic matter. Finally, the samples were transferred into acid-cleaned vials, followed by acid and water rinses to further remove any adsorbed contaminants from the surfaces of the planktic foraminiferal tests. Samples were measured with an inductively coupled plasma-mass spectrometry (ICP-MS) at the State Key Laboratory of Marine Geology, Tongji University, Shanghai. The long-term reproducibility of the Mg/Ca measurements is ± 3.0% (1σ), which is based on 250 analyses of an in-house standard (Mg/Ca = 2.99 mmol/mol). Elemental ratios of Mn/Ca and Al/Ca were analyzed at the same time to monitor any contamination by clays or iron and manganese oxides which could bias the Mg/Ca measurements.

The *G. ruber* Mg/Ca ratios were converted to SST by using an equation developed from tropical Pacific core tops (Lea et al., 2000):

$$SST\ (^{\circ}C) = \ln [Mg/Ca\ (mmol/mol)/0.30]/0.089 \quad (1)$$

We used the Lea et al. (2000) equation for several reasons: (1) The equation of Lea et al. (2000) was developed by using core top samples from the equatorial Pacific which is assumed to reduce regional effects on our Mg/Ca-based SST estimates. (2) Partial dissolution of the planktic foraminiferal tests can result in lower Mg/Ca ratios and thus lower temperature estimates. All core top samples used for the Lea et al. (2000) calibration come from water depths between 2030 and 3200 m water depth. It is therefore likely that these core top samples and our MD06-3047B (2510 m) downcore samples have experienced similar preservation histories. For that reason, the Lea et al. (2000) equation might reduce the influence of water depth on Mg/Ca ratios in our study. (3) The core top samples used by Lea et al. (2000) and our downcore samples were cleaned using a reductive cleaning step. This might minimize the influence of different cleaning methods on the Mg/Ca ratios. The error of the temperature reconstructions is estimated by propagating the errors introduced by the Mg/Ca measurements and the Mg/Ca-temperature calibration, as introduced by Mohtadi et al. (2014). The resulting errors are on average ± 3 °C. Compared to other studies, the relative large error is due to the larger error associated with the Lea et al. (2000) Mg/Ca-temperature calibration.

Our Mg/Ca-based SST record might be problematic in certain intervals because *G. ruber* specimens of the 200–250 μm size fraction have been used for Mg/Ca analysis when no sufficient *G. ruber* individuals were available from the fraction 250–300 μm. To test the effect of different size fractions on the Mg/Ca ratios, *G. ruber* specimens from two different size fractions (250–300 μm and 200–250 μm) were measured for Mg/Ca ratios (Fig. S3). The average Mg/Ca difference between the *G. ruber* individuals of the two different size fractions is ~0.25 mmol/mol which is equivalent to a SST difference of ~0.78 °C. This value is however, within the standard error range (0.5–1 °C) of various published Mg/Ca-temperature equations (Anand et al., 2003; Dekens et al., 2002; Lea et al., 2000).

3.4. Calculation of seawater $\delta^{18}O$ estimates

The $\delta^{18}O$ of seawater and SSS have a linear relationship in the western Pacific (Fairbanks et al., 1997; Gibbons et al., 2014). According to previous studies, the $\delta^{18}O$ of seawater corrected for the influence of continental ice volume ($\delta^{18}O_{sw\text{-}ice}$) is widely used to reconstruct past local/regional hydrological changes (Benway et al., 2006; Schmidt and Spero, 2011). To compute the $\delta^{18}O$ of seawater ($\delta^{18}O_{sw}$), we use the temperature-$\delta^{18}O_{calcite}$ equation of Bemis et al. (1998), which was subsequently supported by a sediment trap study (Thunell et al., 1999):

$$\delta^{18}O_{sw} = [T\ (^{\circ}C) - 16.5 + 4.8 \times \delta^{18}O_{calcite}]/4.8 + 0.27 \quad (2)$$

where $\delta^{18}O_{calcite}$ is the measured $\delta^{18}O$ of *G. ruber* and T is the *G. ruber* based Mg/Ca-derived temperature estimates. Using the same species excludes interfering seasonality and/or habitat effects occurring when proxy data from different planktic foraminiferal groups are used (Leduc et al., 2010; Schmidt and Spero, 2011). The values were then converted to standard mean ocean water (SMOW) by adding 0.27‰. The component of $\delta^{18}O_{sw}$ that is attributed to changes in the local/regional hydrology was then calculated by subtracting the influence of continental ice volume taken from Waelbroeck et al. (2002) and Bintanja et al. (2005) for the periods 450–0 kyr B.P. and 700–0 kyr B.P., respectively. The $\delta^{18}O_{sw\text{-}ice}$ estimates using the data from Waelbroeck et al. (2002) for the period 450–0 kyr B.P. were used to verify the $\delta^{18}O_{sw\text{-}ice}$ estimates using the data from Bintanja et al. (2005). The same method was used to calculate the $\delta^{18}O_{sw\text{-}ice}$ for ODP Site 806B on the Ontong Java Plateau (OJP) (Medina-Elizalde and Lea, 2005), Site MD97-2140 from the center of the WPWP (de Garidel-Thoron et al., 2005) and Site MD06-3018 from the Coral Sea (Russon et al., 2010) for the last 700 kyr. The afore-mentioned method to calculate the $\delta^{18}O_{sw\text{-}ice}$ has been widely used to study changes in the local and regional hydrology of the western Pacific (Oppo and Sun, 2005; Regoli et al., 2015; Schmidt and Spero, 2011; Steinke et al., 2006).

The error in $\delta^{18}O_{sw\text{-}ice}$ was estimated following the method introduced by Mohtadi et al. (2014). Errors are estimated by propagating the error introduced by the $\delta^{18}O_{calcite}$ measurements, the temperature estimates, the $\delta^{18}O$: temperature equation and the removal of the global ice volume (± 0.09‰) (Bintanja et al., 2005; Waelbroeck et al., 2002). This method assumes no covariance among the errors. The resulting average error is ± 0.7‰ for $\delta^{18}O_{sw\text{-}ice}$. Earlier studies reported an error of ± 0.18‰ (ODP 806B; Lea et al., 2000) and ± 0.25‰ (MD97-2140; de Garidel-Thoron et al., 2005) for the $\delta^{18}O$ seawater estimates. However, these studies did not consider the error associated with the removal of the global ice volume effect on the seawater $\delta^{18}O$ values.

4. Results

4.1. Age model

The age model of Core MD06-3047B was developed by visual correlation of the $\delta^{18}O$ record obtained from the benthic foraminifera *F. wuellerstorfi* ($\delta^{18}O_{F.\ wuellerstorfi}$) with the global benthic foraminiferal $\delta^{18}O$ stack LR04 (Lisiecki and Raymo, 2005; Fig. 3). The age model was further refined by the last appearance datum (LAD) of *G. ruber* pink in Core MD06-3047B (at ~156 cm depth downcore). The LAD of pink *G. ruber* at ~120 kyr B.P. is considered to be a reliable biostratigraphical marker in the western Pacific (Thompson et al., 1979). As shown in Fig. 3A, Core MD06-3047B provides a continuous record of the last 700 kyr, covering six full glacial-interglacial cycles. The sedimentation rates range from 0.33 cm/kyr to 6.67 cm/kyr without any obvious differences between glacial and interglacial periods (Fig. 3B).

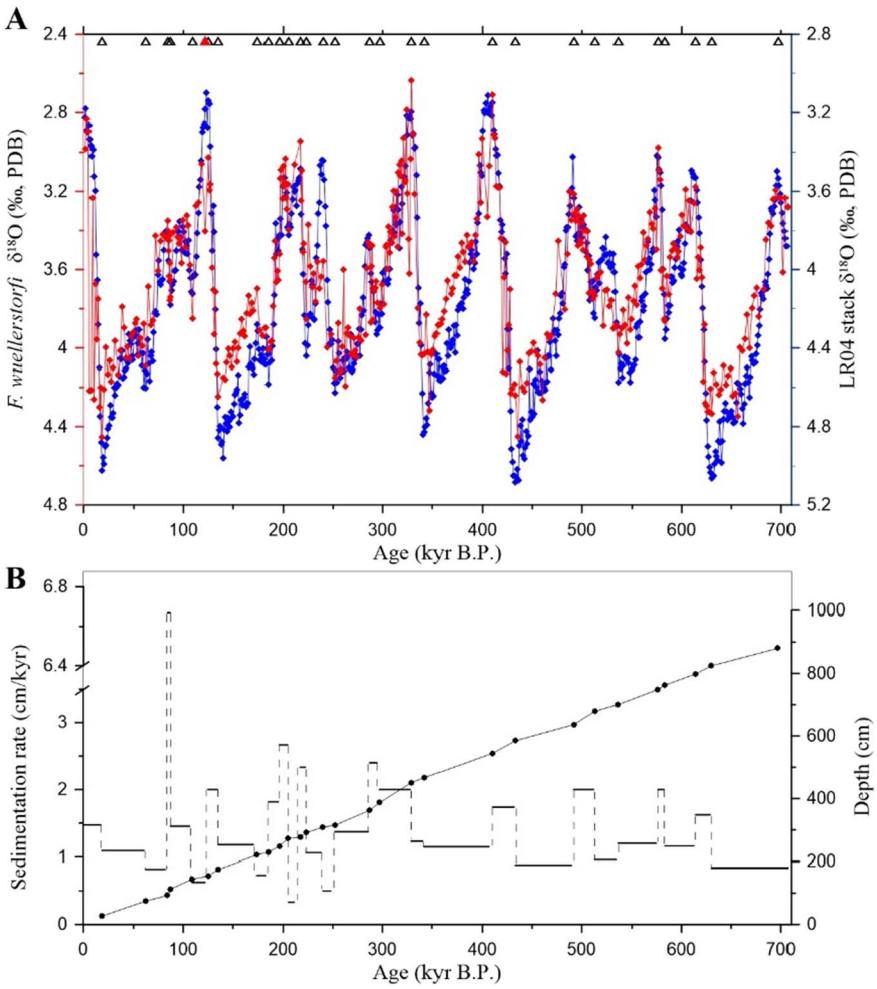

Fig. 3. Age model of Core MD06-3047B. A: the benthic foraminiferal *F. wuellerstorfi* $\delta^{18}O$ (red line) and the global benthic foraminiferal $\delta^{18}O$ stack LR04 (Lisiecki and Raymo, 2005) (blue line), benthic foraminiferal $\delta^{18}O$ tie points (white triangles) and the LAD of *G. ruber* (pink) (red triangle) are also indicated. B: depth-age model and sedimentation rates of sediment Core MD06-3047B. (For interpretation of the references to colour in this figure legend, the reader is referred to the web version of this article.)

4.2. *G. ruber* $\delta^{18}O$

The *G. ruber* $\delta^{18}O$ ($\delta^{18}O_{G.\ ruber}$) record of Core MD06-3047B spans six full glacial-interglacial cycles over the past 700 kyr (Fig. 4A). The amplitude of the glacial-interglacial variations in $\delta^{18}O_{G.\ ruber}$ is on average ~1.27‰. The $\delta^{18}O_{G.\ ruber}$ difference between the LGM and the Holocene is ~1.10‰ (Fig. 4A). This value is similar to values observed in other cores from the WTP but smaller than the average value (~1.30‰) in the ETP (Broecker, 1986). Smaller glacial-interglacial amplitudes in planktic foraminiferal $\delta^{18}O$ in the western Pacific and western Pacific marginal seas compared to e.g. the ETP, were recorded in previous studies (Lea et al., 2000; Li et al., 2010; Steinke et al., 2010; Xiang et al., 2007).

4.3. *G. ruber* Mg/Ca ratios and SST estimates

As shown in Fig. 4B, the *G. ruber* Mg/Ca ratios of Core MD06-3047B show clear glacial-interglacial variations, ranging from ~0.7 to 1.6 mmol/mol (Fig. 4B). The Mg/Ca records yield an average Holocene SST of 28.6 °C and a core top SST of 28.1 °C (Fig. 4C), which is in good agreement with the modern average annual SST for this site (28.1 °C) (Locarnini et al., 2013). The SST difference between the last glaciation and the Holocene is ~2.8 °C (Fig. 4C). Maximum glacial-interglacial differences (~4.5 °C) are recorded at the MIS 12/11 (Termination V) and the MIS 6/5 transitions (Termination II) (Fig. 4C).

4.4. Ice volume-corrected seawater $\delta^{18}O$

As shown in Fig. 4D, the two $\delta^{18}O_{sw\text{-}ice}$ records derived by subtracting the effect of continental ice volume from Waelbroeck et al. (2002) (Fig. 4D, red dash line) and Bintanja et al. (2005) (Fig. 4D, solid green line) are very similar. Therefore, the $\delta^{18}O_{sw\text{-}ice}$ estimates based on simulated global marine isotopes from Bintanja et al. (2005) are reliable and feasible. The $\delta^{18}O_{sw\text{-}ice}$ records of Core MD06-3047B are characterized by lower values during glacials and relative higher values during interglacials over the past 700 kyr (Fig. 4D).

5. Discussion

5.1. WTP glacial-interglacial hydrological changes

Our $\delta^{18}O_{sw\text{-}ice}$ variations suggest that the northern WTP is characterized by lower SSS during glacials and higher SSS during interglacials, most likely indicating more rainfall and thus fresher conditions during glacial periods. We assume that the tropical Pacific exhibits relatively constant temporally and spatially $\delta^{18}O_{sw}$-salinity relationships as suggested by numerical simulation results (Holloway et al., 2016). However, the amplitude of the estimated glacial salinity changes is uncertain because the $\delta^{18}O_{sw\text{-}ice}$ strongly depends on the oxygen isotope composition of the glacial precipitation caused by water vapor transport changes (Oppo et al., 2003; Oppo et al., 2007, and references therein). Nevertheless, the sense of SSS changes is likely to be correct as suggested by previous studies (e.g., Steinke et al., 2006).

In order to assess the hydrological variations across the tropical western Pacific, we compare our results to previous studies from the WTP. For that reason, we calculated the $\delta^{18}O_{sw\text{-}ice}$ records of Core MD97-2140 (de Garidel-Thoron et al., 2005), ODP Hole 806B (Medina-Elizalde and Lea, 2005) and Core MD06-3018 (Russon et al., 2009;

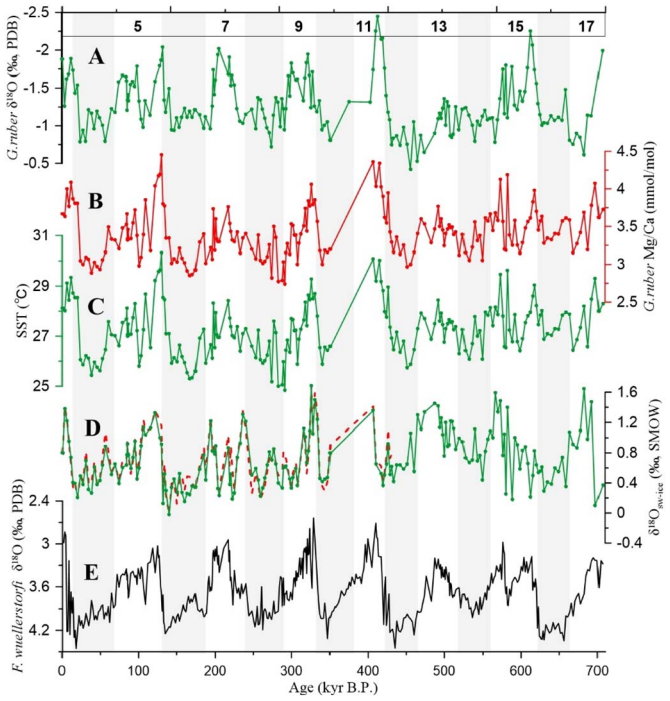

Fig. 4. Planktic foraminiferal proxy records of Core MD06-3047B. A: *G. ruber* (white) $\delta^{18}O$; B: *G. ruber* (white) Mg/Ca; C: *G. ruber* (white) based Mg/Ca-temperature; D: the $\delta^{18}O_{sw\text{-}ice}$ were calculated by using the temperature-$\delta^{18}O_{calcite}$ equation of Bemis et al. (1998). The component of $\delta^{18}O_{sw\text{-}ice}$ that is attributed to changes in the local/regional hydrology was then calculated by subtracting the influence of continental ice volume taken from Waelbroeck et al. (2002) (green solid line) and Bintanja et al. (2005) (red dash line) for the periods 450–0 kyr B.P. and 700–0 kyr B.P., respectively. E: *F. wuellerstorfi* $\delta^{18}O$. The *G. ruber* $\delta^{18}O$ and Mg/Ca records for the time period ~40 to ~35 kyr B.P. are not well constrained because insufficient *G. ruber* shells were available for reliable measurements. The average error of the SST and $\delta^{18}O_{sw\text{-}ice}$ estimates is ± 3 °C and ± 0.7‰, respectively (see details in Sections 3.3 and 3.4). (For interpretation of the references to colour in this figure legend, the reader is referred to the web version of this article.)

Russon et al., 2010) following our approach outlined in Section 3.4. The original datasets of these cores are detailed in Table 1. Our results are in good agreement with other $\delta^{18}O_{sw\text{-}ice}$ records from the western Pacific: the $\delta^{18}O_{sw\text{-}ice}$ records of Cores MD06-3047B (this study), MD97-2140 (de Garidel-Thoron et al., 2005), ODP Hole 806B (Medina-Elizalde and Lea, 2005) and Core MD06-3018 (Russon et al., 2009; Russon et al., 2010), which all exhibit generally consistent glacial-interglacial variations (Fig. 5). All records are characterized by lower $\delta^{18}O_{sw\text{-}ice}$ values (lower SSS and thus most likely higher rainfall) during glacial periods. This indicates that both the northern WTP and the western equatorial Pacific simultaneously experienced fresher and wetter conditions during glacial periods. Next, we are trying to discuss about the possible reason(s) for the glacial freshening of the WTP.

Although Rincón-Martínez et al. (2010) suggested a glacial northward shift of ITCZ in eastern equatorial Pacific, paleoclimate records from the Cariaco Basin and Colombia Basin invoke a southward displacement of the ITCZ during glacial periods in the tropical Atlantic and tropical eastern Pacific (Mora and Martínez, 2005; Schmidt and Spero, 2011; Yarincik et al., 2000). Model simulations also support southward shift of ITCZ because of the Northern Hemisphere cooling during glacial periods (Broccoli et al., 2006; Chiang and Bitz, 2005). However, southward shift of the ITCZ might explain very well the glacial freshening in the equatorial WTP (Schmidt and Spero, 2011; Schneider et al., 2014) but is most likely not an appropriate mechanism for explaining the lower salinity in the northern WTP during glacial periods. For that reason, we suggest a complex pattern of tropical atmospheric circulation responsible for the hydrological variations in the WTP, most likely including shifts in the ITCZ and zonal shifts associated with ENSO variability (see below).

5.2. Forcing mechanisms of WTP hydrological variations

We performed a spectral analysis on the $\delta^{18}O_{sw\text{-}ice}$ records of Core MD06-3047B over the past 700 kyr (Fig. 6A). Spectral analysis shows that $\delta^{18}O_{sw\text{-}ice}$ records display prominent periodicities corresponding to the eccentricity (100 kyr) and obliquity (41 kyr) bands (Fig. 6A), which are characteristic of glacial-interglacial cycles (Lisiecki and Raymo, 2005). The presence of 100 kyr and 40 kyr cycles of our $\delta^{18}O_{sw\text{-}ice}$ records might indicate that the hydrological changes in the WTP are correlated to high latitude insolation variations or changes in continental ice volume (Huybers and Wunsch, 2005; Rutherford and D'Hondt, 2000). Here we propose possible forcing mechanisms for WTP hydrological variations by comparing our results with some modeling results (DiNezio et al., 2011; DiNezio and Tierney, 2013; Zhang and Delworth, 2005).

Weakening of the AMOC might have caused changes in tropical atmospheric circulation during glacial episodes (Mohtadi et al., 2014). Simulation results from a global coupled ocean-atmosphere model indicate La Niña-like conditions and a stronger Walker circulation in the northern tropical Pacific and a southward shift of the ITCZ due to a substantial weakening of the AMOC (Zhang and Delworth, 2005). According to these simulations, we speculate that the stronger Walker circulation over the tropical Pacific and the southward shift of the ITCZ might have resulted in more precipitation in the northern and southern

Table 1
SST records used to calculate the west-east tropical Pacific zonal SST gradients and $\delta^{18}O_{sw\text{-}ice}$ records.

Location	Site/record	Parameter	Latitude	Longitude	Depth (m)	References
West Pacific	ODP 806B	Mg/Ca SST $\delta^{18}O$ (p)	0° 19′ N	159° 22′ E	2520	Medina-Elizalde and Lea (2005)
	MD97–2140	Mg/Ca SST $\delta^{18}O$ (p)	2° 02′ N	141° 46′ E	2547	de Garidel-Thoron et al. (2005)
	MD06–3018	Mg/Ca SST $\delta^{18}O$ (p) $\delta^{18}O$ (b)	23° 00′ S	166° 09′ E	2470	Russon et al. (2010) Russon et al. (2009)
	MD06-3047B	Mg/Ca SST $\delta^{18}O$ (b)	17° 00′ N	124° 48′ E	2510	This study
East Pacific	ODP 846	$U^{k'}_{37}$ SST $\delta^{18}O$ (b)	3° 05′ S	90° 49′ W	3296	Liu and Herbert (2004) Mix et al. (1995)
	ODP 1239	$U^{k'}_{37}$ SST $\delta^{18}O$ (b)	0° 40′ S	82° 05′ W	1414	Dyez et al. (2016)
	TR163-19	Mg/Ca SST $\delta^{18}O$ (p)	2° 16′ N	90° 57′ W	2348	Lea et al. (2000)

* b = benthic, p = planktonic, SST = sea surface temperature.

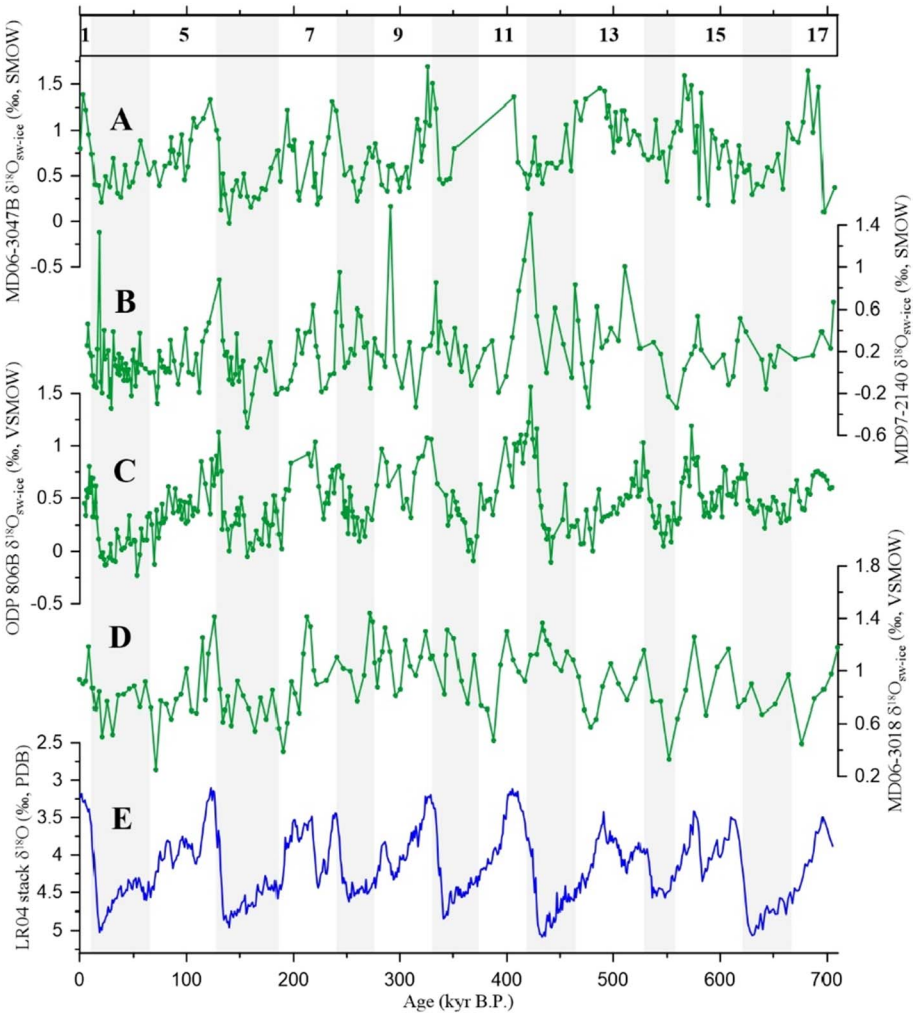

Fig. 5. Comparison of $\delta^{18}O_{sw\text{-}ice}$ records. A: $\delta^{18}O_{sw\text{-}ice}$ records of Core MD06-3047B (this study); B: $\delta^{18}O_{sw\text{-}ice}$ records of Core MD97-2140 (de Garidel-Thoron et al., 2005); C: $\delta^{18}O_{sw\text{-}ice}$ records of ODP Hole 806B (Medina-Elizalde and Lea, 2005); D: $\delta^{18}O_{sw\text{-}ice}$ records of Core MD06-3018 (Russon et al., 2009; Russon et al., 2010); E: LR04 benthic stack (Lisiecki and Raymo, 2005).

tropical WTP during glacial periods (Broccoli et al., 2006; Schmidt and Spero, 2011). The glacial freshening at ODP Hole 806B (Medina-Elizalde and Lea, 2005) has been explained by a southern shift of the Pacific ITCZ due to the weakening of the AMOC (Schmidt and Spero, 2011). Whereas the same model study indicated El Niño-like condition in the southern WTP and La Niña-like condition in the northern WTP under the condition of weakened AMOC (Zhang and Delworth, 2005). Those results are in contrast to some other model studies which show that the thermal state of the WTP changes as a whole (Zhu et al., 2017). However, Zhang and Delworth's (2005) simulation results with weakened AMOC were derived using modern boundary conditions rather than glacial boundary conditions. For that reason, there might be other forcing mechanisms involved driving glacial WTP hydrological variations in the tropical Pacific.

The exposure of large land masses due to changes in sea level as the result of the growth of continental ice sheets mainly in the northern high latitudes might have also contributed to WTP precipitation and SSS changes during glacials (Clark and Mix, 2002; DiNezio et al., 2011). An ensemble of several coordinated coupled climate model simulations reveal a large reduction of precipitation over the exposed Maritime Continent (i.e. parts of SE Asia in particular the glacial exposed Sunda shelf and the islands of Indonesia and the Philippines) but fresher conditions in the WTP during the LGM (DiNezio et al., 2011; DiNezio and Tierney, 2013). This has been explained by a stronger Pacific Walker circulation as a response to either a stronger SST gradient or changes in the hydrological cycle over the tropical Pacific (DiNezio et al., 2011; DiNezio and Tierney, 2013). Accordingly, we infer that the growth and decay of ice sheets have exerted a significant influence on the hydroclimate over the WTP through the associated changes in global sea level and thus the exposure of large land masses (DiNezio et al., 2011; DiNezio and Tierney, 2013).

5.3. The mean thermal state over tropical Pacific

The zonal SST asymmetry between the warm west and cool east Pacific is an essential feature of ENSO (Picaut et al., 1996). A strong zonal gradient is associated with La Niña conditions, while a weak zonal gradient indicates El Niño conditions (Picaut et al., 1996). In order to explore the evolution of the mean background state of the tropical Pacific, we estimated the tropical zonal SST gradient for the last 700 kyr using SST records from the WTP and ETP (Fig. 7). To calculate the tropical zonal SST gradient, we used the Mg/Ca-based SST data from Core MD06-3047B and Mg/Ca-based SST data from three other studies from the western Pacific as well as three SST records from the eastern Pacific cold tongue (Table 1). The age models of the seven cores used are generally consistent to each other as shown by the $\delta^{18}O$ records (Fig. 7D). In addition, we used two long-term $U^{k'}_{37}$-based SST records from the eastern Pacific cold tongue due to the lack of long-term Mg/Ca-based SST from the eastern Pacific. Previous studies suggested that $U^{k'}_{37}$-based SST reconstructions agree well with Mg/Ca-based SST records in the eastern tropical Pacific (Leduc et al., 2007). To test if the zonal gradient SST reconstructions are biased by the use of SST estimates of different plankton groups, we estimated the difference between the western and eastern Pacific by only using Mg/Ca-based SST

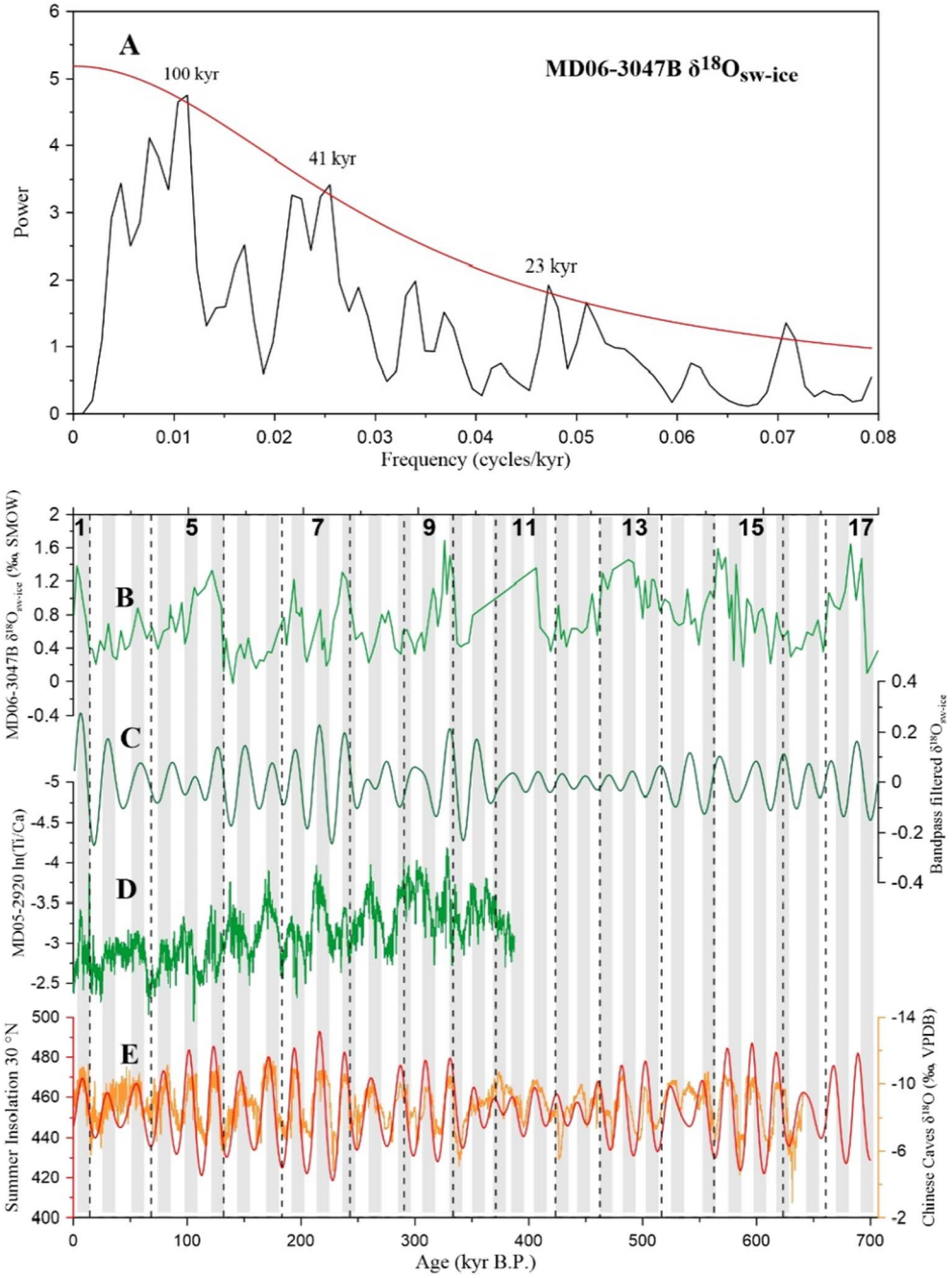

Fig. 6. The comparison of orbital-scale precipitation pattern between the WTP and continental East Asia over the past 700 kyr. A: spectrum of $\delta^{18}O_{sw\text{-}ice}$. REDFIT spectral analysis (Schulz and Mudelsee, 2002) of $\delta^{18}O_{sw\text{-}ice}$ in Core MD06-3047B using the PAST software (Hammer et al., 2001). The red line indicates the 90% confidence interval. B: $\delta^{18}O_{sw\text{-}ice}$ record of Core MD06-3047B. C: band-pass filtered $\delta^{18}O_{sw\text{-}ice}$ record of Core MD06-3047B using a frequency of 0.0454 kyr^{-1} to isolate the 23-kyr component. D: the ln(Ti/Ca) record of Core MD05-2920. E: summer insolation at 30°N (Laskar et al., 2004) superimposed on the speleothem $\delta^{18}O$ records from four caves in China (Cheng et al., 2016). (For interpretation of the references to colour in this figure legend, the reader is referred to the web version of this article.)

estimates (Fig. 7C, green line). As shown in Fig. 7C, the trend of all the records is very similar, suggesting no bias due to the use of SST estimates of different plankton groups. Our estimates show that the zonal SST gradient over the tropical Pacific was enhanced during glacial periods compared to interglacial periods. We therefore suggest that a larger tropical zonal SST gradient indicate more La Niña-like conditions during glacial intervals.

Several previous studies support our concept for more La Niña-like conditions during glacial periods. Planktic foraminiferal abundance data indicate a steeper east-west thermocline slope along the equator. This result suggests that the Walker circulation was intensified during the LGM (Andreasen and Ravelo, 1997). A larger zonal SST gradient based on Mg/Ca-based SST reflects enhanced trade winds during glacial episodes, analogous to La Niña-like conditions (Lea et al., 2000; Zhang et al., 2016). Planktic mineralogical assemblages and stable isotopes indicate a stronger SST meridional gradient and a stronger advection of Peru Current waters to the ETP compared to the present, suggesting La Niña-like conditions in the ETP during the last glaciation (Martínez et al., 2003). In addition, a coupled climate model simulation suggests the westward shift of precipitation in the WTP, indicating a La Niña-like mean response under glacial conditions (Kim et al., 2002). Although several studies propose El Niño-like conditions during glacial intervals (Koutavas and Joanides, 2012; Koutavas et al., 2002; Stott et al., 2002), our results support the idea of La Niña-like conditions during glacial periods. We therefore suggest that the glacial La Niña-like conditions might contribute to a strengthening of the Walker circulation, resulting in more rainfall in our study area.

5.4. Precipitation patterns in the WTP and East Asia on orbital timescales

Results of the spectral analysis also display a 23-kyr component, which corresponds to the precession cycle (Fig. 6A). The filtered 23-kyr

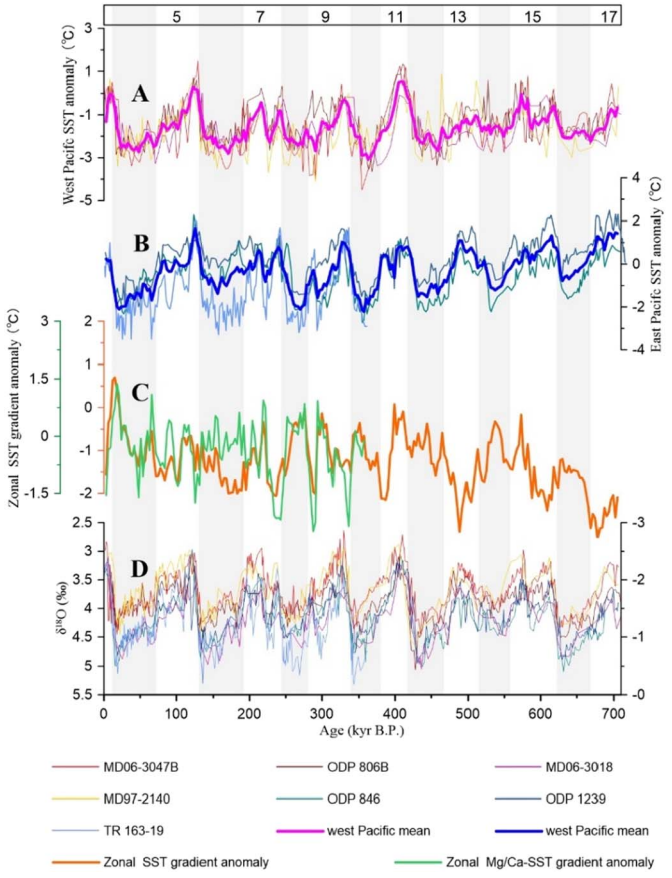

Fig. 7. Reconstructed zonal SST gradient across the tropical Pacific during the last 700 kyr. A and B: SST reconstructions from four western and three eastern Pacific coring sites, respectively (see Table 1 for list for details). SST in A and B is expressed as anomaly relative to the Holocene (11.7–0 kyr B.P.). The thick magenta and blue lines represent the average SST anomalies for the western and eastern Pacific, respectively, by averaging non-overlapping 3-kyr bins. C: zonal SST gradient anomalies relative to the Holocene values. The orange line represents the SST difference of the western and eastern Pacific based on the Mg/Ca-based and $U^{k'}_{37}$-based SSTs. The green line represents the zonal SST gradient by using Mg/Ca-based SSTs only. D: planktic and benthic foraminiferal $\delta^{18}O$ records used to establish the age models for each cores (also see Table 1 for list of cores). All $\delta^{18}O$ records are reported relative to the PDB or Vienna Pee Dee Belemnite (VPDB) according to original references (Table 1). (For interpretation of the references to colour in this figure legend, the reader is referred to the web version of this article.)

component of Core MD06-3047B $\delta^{18}O_{sw\text{-}ice}$ records is shown in Fig. 6C. Higher values and thus lower precipitation correspond to summer insolation maximum at 30°N (Fig. 6C and E). Sedimentological data of a core recovered off the Philippine island of Mindanao also suggest that precipitation was lower in the WTP during Northern Hemisphere summer insolation maxima (or southern summer insolation minimum) (Kissel et al., 2010; Tachikawa et al., 2011; Fig. 6D). Tachikawa et al. (2011) suggested that precipitation over Papua New Guinea is controlled by the interhemispheric insolation contrast and thus an interhemispheric anti-phase precipitation pattern on orbital timescales. However, the same rainfall patterns in the northwestern equatorial Pacific (this study; Kissel et al., 2010) indicate in-phase pattern of rainfall variability in the south and north of equator over the WTP. In contrast to the records of the WTP, speleothem $\delta^{18}O$ records of Chinese caves show enhanced East Asian summer monsoon precipitation during Northern Hemisphere summer insolation maxima (Cheng et al., 2016; Fig. 6E).

Our results support the idea that there may exist an opposite trend in precipitation between the East Asian landmass and the WTP due to the redistribution of energy controlled by precession (Braconnot et al., 2008; Kissel et al., 2010). The modeling results indicated that the increased warming in the Northern Hemisphere will strengthen the interhemispheric gradient and increase land-sea contrast with large increase of tropospheric warming over the Tibetan plateau (Braconnot et al., 2008). These processes contributed to the advection of moist air from the ocean into the monsoon regions (Braconnot et al., 2008). The strengthening of the monsoon flow will cause the increased moisture divergence over the ocean and increased moisture convergence over land (Braconnot et al., 2008). The change in the atmospheric circulation will result in an anti-phase precipitation pattern between the WTP and continent East Asia (Braconnot et al., 2008). However, more studies about the relationship between the East Asia and the WTP hydrological variability on orbital timescales are needed to understand the complex rainfall patterns and associated feedbacks in the tropical Pacific and East Asia.

6. Conclusions

Through the reconstruction of SST and $\delta^{18}O_{sw\text{-}ice}$ records in the northern WTP and comparison with those from other sites in the central, southern WTP, and ETP, we draw the following conclusions regarding the hydrological variations in the WTP over the past 700 kyr.

(1) The WTP experienced significant hydrologic changes on glacial-interglacial timescales. The $\delta^{18}O_{sw\text{-}ice}$ records are characterized by higher values (lower SSS and thus most likely higher precipitation) during glacial periods.
(2) The variability in the hydroclimate over the tropical Pacific might be controlled by exposure of the Maritime Continent due to sea level changes and/or a weakened AMOC during glacial periods through changes in the Pacific Walker circulation and/or the migration of ITCZ. Our results support the idea that climate change in the northern high latitude strongly influences on the hydroclimate in the tropics.
(3) Our results suggest an enhanced tropical zonal Pacific SST gradient during glacial periods, indicating La Niña-like conditions. La Niña-like conditions might also have contributed to lower SSS and thus higher rainfall in the WTP during glacials.
(4) Our results support the idea of an opposite trend in precipitation between continental East Asia and the WTP on orbital timescales, which may be due to the redistribution of energy controlled by precession and associated variations in monsoon flow according to previous model simulation.

Acknowledgments

We thank the chief scientist Carlo Laj, the captain and the crew of *R/V* Marion Dufresne, and the French Polar Institute for their effort and support during the IMAGES XIV-MD155-Marco Polo 2 cruise. We would like to thank Ann Holbourn and one anonymous reviewer for their constructive comments, which helped to improve the quality of our manuscript. This study was supported by the Open Fund of Qingdao National Laboratory for Marine Science and Technology (grant no. QNLM2016ORP0205), National Natural Science Foundation of China (grant nos. 41230959, 41106042, 41576051, 41776065, 41576050), and National Special Project for Global Change and Air-Sea Interaction (grant no. GASI-GEOGE-04).

Appendix A. Supplementary data

Supplementary data to this article can be found online at https://doi.org/10.1016/j.palaeo.2017.12.039.

References

Anand, P., Elderfield, H., Conte, M.H., 2003. Calibration of Mg/Ca thermometry in planktonic foraminifera from a sediment trap time series. Paleoceanography 18.

http://dx.doi.org/10.1029/2002PA000846.
Andreasen, D.J., Ravelo, A.C., 1997. Tropical Pacific Ocean thermocline depth reconstructions for the Last Glacial Maximum. Paleoceanography 12, 395–413.
Beaufort, L., de Garidel-Thoron, T., Mix, A.C., Pisias, N.G., 2001. ENSO-like forcing on oceanic primary production during the Late Pleistocene. Science 293, 2440–2444.
Bemis, B.E., Spero, H.J., Bijma, J., Lea, D.W., 1998. Reevaluation of the oxygen isotopic composition of planktonic foraminifera: experimental results and revised paleotemperature equations. Paleoceanography 13, 150–160.
Benway, H.M., Mix, A.C., Haley, B.A., Klinkhammer, G.P., 2006. Eastern Pacific Warm Pool paleosalinity and climate variability: 0–30 kyr. Paleoceanography 21. http://dx.doi.org/10.1029/2005PA001208.
Berger, W.H., Bonneau, M.C., Parker, F.L., 1982. Foraminifera on the deep-sea floor-lysocline and dissolution rate. Oceanol. Acta 5, 249–258.
Bintanja, R., van de Wal, R.S., Oerlemans, J., 2005. Modelled atmospheric temperatures and global sea levels over the past million years. Nature 437, 125–128.
Boyle, E.A., Keigwin, L.D., 1985/1986. Comparison of Atlantic and Pacific paleochemical records for the last 215,000 years: changes in deep ocean circulation and chemical inventories. Earth Planet. Sci. Lett. 76, 135–150.
Braconnot, P., Marzin, C., Gregoire, L., Mosquet, E., Marti, O., 2008. Monsoon response to changes in Earth's orbital parameters: comparisons between simulations of the Eemian and of the Holocene. Clim. Past 4, 281–294.
Broccoli, A.J., Dahl, K.A., Stouffer, R.J., 2006. Response of the ITCZ to Northern Hemisphere cooling. Geophys. Res. Lett. 33. http://dx.doi.org/10.1029/2005GL024546.
Broecker, W.S., 1986. Oxygen isotope constraints on surface ocean temperatures. Quat. Res. 26, 121–134.
Cane, M.A., 1998. A role for the tropical Pacific. Science 282, 59–61.
Carre, M., Sachs, J.P., Purca, S., Schauer, A.J., Braconnot, P., Falcon, R.A., Julien, M., Lavallee, D., 2014. Holocene history of ENSO variance and asymmetry in the eastern tropical Pacific. Science 345, 1045–1048.
Cheng, H., Edwards, R.L., Sinha, A., Spotl, C., Yi, L., Chen, S., Kelly, M., Kathayat, G., Wang, X., Li, X., Kong, X., Wang, Y., Ning, Y., Zhang, H., 2016. The Asian monsoon over the past 640,000 years and ice age terminations. Nature 534, 640–646.
Chiang, J.C.H., Bitz, C.M., 2005. Influence of high latitude ice cover on the marine Intertropical Convergence Zone. Clim. Dyn. 25, 477–496.
Clark, P.U., Mix, A.C., 2002. Ice sheets and sea level of the Last Glacial Maximum. Quat. Sci. Rev. 21, 1–7.
Dekens, P.S., Lea, D.W., Pak, D.K., Spero, H.J., 2002. Core top calibration of Mg/Ca in tropical foraminifera: refining paleotemperature estimation. Geochem. Geophys. Geosyst. 3 (4), 1–29.
Delcroix, T., Henin, C., Porte, V., Arkin, P., 1996. Precipitation and sea-surface salinity in the tropical Pacific Ocean. Deep-Sea Res. I Oceanogr. Res. Pap. 43, 1123–1141.
Deplazes, G., Lückge, A., Peterson, L.C., Timmermann, A., Hamann, Y., Hughen, K.A., Röhl, U., Laj, C., Cane, M.A., Sigman, D.M., Haug, G.H., 2013. Links between tropical rainfall and North Atlantic climate during the last glacial period. Nat. Geosci. 6, 213–217.
Deser, C., Wallace, J.M., 1990. Large-scale atmospheric circulation features of warm and cold episodes in the tropical Pacific. J. Clim. 3, 1254–1281.
DiNezio, P.N., Tierney, J.E., 2013. The effect of sea level on glacial Indo-Pacific climate. Nat. Geosci. 6, 485–491.
DiNezio, P.N., Clement, A., Vecchi, G.A., Soden, B., Broccoli, A.J., Otto-Bliesner, B.L., Braconnot, P., 2011. The response of the Walker circulation to Last Glacial Maximum forcing: implications for detection in proxies. Paleoceanography 26. http://dx.doi.org/10.1029/2010PA002083.
Dyez, K.A., Ravelo, A.C., Mix, A.C., 2016. Evaluating drivers of Pleistocene eastern tropical Pacific sea surface temperature. Paleoceanography 31, 1054–1069.
Fairbanks, R.G., Evans, M.N., Rubenstone, J.L., Mortlock, R.A., Broad, K., Moore, M.D., Charles, C.D., 1997. Evaluating climate indices and their geochemical proxies measured in corals. Coral Reefs 16, S93–S100.
Fine, R.A., Lukas, R., Bingham, F.M., Warner, M.J., Gammon, R.H., 1994. The western equatorial Pacific: a water mass crossroads. J. Geophys. Res. Oceans 99, 25063–25080.
Fleitmann, D., Burns, S.J., Mangini, A., Mudelsee, M., Kramers, J., Villa, I., Neff, U., Al-Subbary, A.A., Buettner, A., Hippler, D., Matter, A., 2007. Holocene ITCZ and Indian monsoon dynamics recorded in stalagmites from Oman and Yemen (Socotra). Quat. Sci. Rev. 26, 170–188.
Ford, H.L., Ravelo, A.C., Polissar, P.J., 2015. Reduced El Niño-Southern Oscillation during the Last Glacial Maximum. Science 347, 255–258.
de Garidel-Thoron, T.D., Rosenthal, Y., Bassinot, F., Beaufort, L., 2005. Stable sea surface temperatures in the western Pacific warm pool over the past 1.75 million years. Nature 433, 294–298.
Gibbons, F.T., Oppo, D.W., Mohtadi, M., Rosenthal, Y., Cheng, J., Liu, Z., Linsley, B.K., 2014. Deglacial $\delta^{18}O$ and hydrologic variability in the tropical Pacific and Indian Oceans. Earth Planet. Sci. Lett. 387, 240–251.
Groetsch, J., Wu, G., Berger, W.H., 1991. Carbonate saturation cycles in the western equatorial Pacific. In: Cycles and Events in Stratigraphy. Springer, Heidelberg, pp. 110–125.
Halpert, M.S., Ropelewski, C.F., 1992. Surface temperature patterns associated with the Southern Oscillation. J. Clim. 5, 577–593.
Hammer, Ø., Harper, D.A.T., Ryan, P.D., 2001. PAST: paleontological statistics software package for education and data analysis. Palaeontol. Electron. 4, 1–9.
Hilde, T.W.C., Lee, C.S., 1984. Origin and evolution of the West Philippine Basin: a new interpretation. Tectonophysics 102, 85–104.
Hoerling, M.P., Hurrell, J.W., Xu, T., 2001. Tropical origins for recent North Atlantic climate change. Science 292, 90–92.
Holloway, M.D., Sime, L.C., Singarayer, J.S., Tindall, J.C., Valdes, P.J., 2016. Reconstructing paleosalinity from $\delta^{18}O$: coupled model simulations of the Last Glacial Maximum, Last Interglacial and Late Holocene. Quat. Sci. Rev. 131, 350–364.
Huybers, P., Wunsch, C., 2005. Obliquity pacing of the late Pleistocene glacial terminations. Nature 434, 491–494.
Jiang, F.Q., Zhou, Y., Nan, Q.Y., Zhou, Y., Zheng, X.F., Li, T.G., Li, A.C., Wang, H.L., 2016. Contribution of Asian dust and volcanic material to the western Philippine Sea over the last 220 kyr as inferred from grain size and Sr-Nd isotopes. J. Geophys. Res. Oceans 121, 6911–6928.
Kim, S.J., Flato, G.M., Boer, G.J., McFarlane, N.A., 2002. A coupled climate model simulation of the Last Glacial Maximum, part 1: transient multi-decadal response. Clim. Dyn. 19, 515–537.
Kissel, C., Laj, C., Kienast, M., Bolliet, T., Holbourn, A., Hill, P., Kuhnt, W., Braconnot, P., 2010. Monsoon variability and deep oceanic circulation in the western equatorial Pacific over the last climatic cycle: insights from sedimentary magnetic properties and sortable silt. Paleoceanography 25. http://dx.doi.org/10.1029/2010PA001980.
Koutavas, A., Joanides, S., 2012. El Niño-Southern Oscillation extrema in the Holocene and Last Glacial Maximum. Paleoceanography 27. http://dx.doi.org/10.1029/2012PA002378.
Koutavas, A., Lynch-Stieglitz, J., Marchitto Jr., T.M., Sachs, J.P., 2002. El Niño-like pattern in ice age tropical Pacific sea surface temperature. Science 297, 226–230.
Laskar, J., Robutel, P., Joutel, F., Gastineau, M., Correia, A.C.M., Levrard, B., 2004. A long-term numerical solution for the insolation quantities of the Earth. Astron. Astrophys. 428, 261–285.
Lea, D.W., Pak, D.K., Spero, H.J., 2000. Climate impact of late Quaternary equatorial Pacific sea surface temperature variations. Science 289, 1719–1724.
Leduc, G., Vidal, L., Tachikawa, K., Rostek, F., Sonzogni, C., Beaufort, L., Bard, E., 2007. Moisture transport across Central America as a positive feedback on abrupt climatic changes. Nature 445, 908–911.
Leduc, G., Vidal, L., Cartapanis, O., Bard, E., 2009a. Modes of eastern equatorial Pacific thermocline variability: implications for ENSO dynamics over the last glacial period. Paleoceanography 24. http://dx.doi.org/10.1029/2008PA001701.
Leduc, G., Vidal, L., Tachikawa, K., Bard, E., 2009b. ITCZ rather than ENSO signature for abrupt climate changes across the tropical Pacific? Quat. Res. 72, 123–131.
Leduc, G., Schneider, R., Kim, J.H., Lohmann, G., 2010. Holocene and Eemian sea surface temperature trends as revealed by alkenone and Mg/Ca paleothermometry. Quat. Sci. Rev. 29, 989–1004.
Li, T., Zhao, J., Sun, R., Chang, F., Sun, H., 2010. The variation of upper ocean structure and paleoproductivity in the Kuroshio source region during the last 200 kyr. Mar. Micropaleontol. 75, 50–61.
Lisiecki, L., Raymo, M., 2005. A Pliocene-Pleistocene stack of 57 globally distributed benthic $\delta^{18}O$ records. Paleoceanography 20. http://dx.doi.org/10.1029/2004PA001071.
Liu, Z., Herbert, T.D., 2004. High-latitude influence on the eastern equatorial Pacific climate in the early Pleistocene epoch. Nature 427, 720–723.
Liu, Z., Lu, Z., Wen, X., Otto-Bliesner, B.L., Timmermann, A., Cobb, K.M., 2014. Evolution and forcing mechanisms of El Niño over the past 21,000 years. Nature 515, 550–553.
Locarnini, R.A., Mishonov, A.V., Antonov, J.I., Boyer, T.P., Garcia, H.E., Baranova, O.K., Zweng, M.M., Paver, C.R., Reagan, J.R., Johnson, D.R., Hamilton, M., Seidov, D., 2013. World Ocean Atlas 2013, volume 1: temperature. Technical Ed. In: Levitus, S., Mishonov, A. (Eds.), NOAA Atlas NESDIS 73, (40 pp).
Lyon, B., Cristi, H., Verceles, E.R., Hilario, F.D., Abastillas, R., 2006. Seasonal reversal of the ENSO rainfall signal in the Philippines. Geophys. Res. Lett. 33. http://dx.doi.org/10.1029/2006GL028182.
Martin, P.A., Lea, D.W., 2002. A simple evaluation of cleaning procedures on fossil benthic foraminiferal Mg/Ca. Geochem. Geophys. Geosyst. 3, 1–8.
Martínez, I., Keigwin, L., Barrows, T.T., Yokoyama, Y., Southon, J., 2003. La Niña-like conditions in the eastern equatorial Pacific and a stronger Choco jet in the northern Andes during the last glaciation. Paleoceanography 18. http://dx.doi.org/10.1029/2002PA000877.
Medina-Elizalde, M., Lea, D.W., 2005. The mid-Pleistocene transition in the tropical Pacific. Science 310, 1009–1012.
Mix, A.C., Le, J., Shackleton, N.J., 1995. Benthic foraminiferal stable isotope stratigraphy of site 846: 0–1.8 Ma. In: Proceedings of the Ocean Drilling Program, Scientific Results. 138. pp. 839–847.
Mohtadi, M., Prange, M., Oppo, D.W., De Pol-Holz, R., Merkel, U., Zhang, X., Steinke, S., Luckge, A., 2014. North Atlantic forcing of tropical Indian Ocean climate. Nature 509, 76–80.
Mora, G., Martínez, J.I., 2005. Sedimentary metal ratios in the Colombia Basin as indicators for water balance change in northern South America during the past 400,000 years. Paleoceanography 20. http://dx.doi.org/10.1029/2005PA001132.
Oppo, D.W., Sun, Y., 2005. Amplitude and timing of sea-surface temperature change in the northern South China Sea: dynamic link to the East Asian monsoon. Geology 33, 785–788.
Oppo, D.W., Linsley, B.K., Rosenthal, Y., Dannenmann, S., Beaufort, L., 2003. Orbital and suborbital climate variability in the Sulu Sea, western tropical Pacific. Geochem. Geophys. Geosyst. 4, 1–20.
Oppo, D.W., Schmidt, G.A., LeGrande, A.N., 2007. Seawater isotope constraints on tropical hydrology during the Holocene. Geophys. Res. Lett. 34. http://dx.doi.org/10.1029/2007GL030017.
Otto-Bliesner, B.L., Brady, E.C., Shin, S.I., Liu, Z., Shields, C., 2003. Modeling El Niño and its tropical teleconnections during the last glacial-interglacial cycle. Geophys. Res. Lett. 30. http://dx.doi.org/10.1029/2003GL018553.
Picaut, J., Ioualalen, M., Menkes, C., Delcroix, T., McPhaden, M.J., 1996. Mechanism of the zonal displacements of the Pacific warm pool: implications for ENSO. Science 274, 1486–1489.
Regoli, F., Garidel-Thoron, T., Tachikawa, K., Jian, Z., Ye, L., Droxler, A.W., Lenoir, G.,

Crucifix, M., Barbarin, N., Beaufort, L., 2015. Progressive shoaling of the equatorial Pacific thermocline over the last eight glacial periods. Paleoceanography 30, 439–455.

Rincón-Martínez, D., Lamy, F., Contreras, S., Leduc, G., Bard, E., Saukel, C., Blanz, T., Mackensen, A., Tiedemann, R., 2010. More humid interglacials in Ecuador during the past 500 kyr linked to latitudinal shifts of the equatorial front and the Intertropical Convergence Zone in the eastern tropical Pacific. Paleoceanography 25. http://dx.doi.org/10.1029/2009PA001868.

Ropelewski, C.F., Halpert, M.S., 1987. Global and regional scale precipitation patterns associated with the El Niño/Southern Oscillation. Mon. Weather Rev. 115, 1606–1626.

Russon, T., Elliot, M., Kissel, C., Cabioch, G., De Deckker, P., Corrège, T., 2009. Middle-late Pleistocene deep water circulation in the southwest subtropical Pacific. Paleoceanography 24. http://dx.doi.org/10.1029/2009PA001755.

Russon, T., Elliot, M., Sadekov, A., Cabioch, G., Corrège, T., De Deckker, P., 2010. Inter-hemispheric asymmetry in the early Pleistocene Pacific warm pool. Geophys. Res. Lett. 37. http://dx.doi.org/10.1029/2010GL043191.

Rutherford, S., D'Hondt, S., 2000. Early onset and tropical forcing of 100,000-year Pleistocene glacial cycles. Nature 408, 72–75.

Sagawa, T., Yokoyama, Y., Ikehara, M., Kuwae, M., 2012. Shoaling of the western equatorial Pacific thermocline during the last glacial maximum inferred from multispecies temperature reconstruction of planktonic foraminifera. Palaeogeogr. Palaeoclimatol. Palaeoecol. 346-347, 120–129.

Schmidt, M.W., Spero, H.J., 2011. Meridional shifts in the marine ITCZ and the tropical hydrologic cycle over the last three glacial cycles. Paleoceanography 26. http://dx.doi.org/10.1029/2010PA001976.

Schneider, T., Bischoff, T., Haug, G.H., 2014. Migrations and dynamics of the intertropical convergence zone. Nature 513, 45–53.

Schulz, M., Mudelsee, M., 2002. REDFIT: estimating red-noise spectra directly from unevenly space paleoclimate time series. Comput. Geosci. 28, 421–426.

Steinke, S., Chiu, H.-Y., Yu, P.-S., Shen, C.-C., Erlenkeuser, H., Löwemark, L., Chen, M.-T., 2006. On the influence of sea level and monsoon climate on the southern South China Sea freshwater budget over the last 22,000 years. Quat. Sci. Rev. 25, 1475–1488.

Steinke, S., Mohtadi, M., Groeneveld, J., Lin, L.-C., Löwemark, L., Chen, M.-T., Rendle-Bühring, R., 2010. Reconstructing the southern South China Sea upper water column structure since the Last Glacial Maximum: implications for the East Asian winter monsoon development. Paleoceanography 25. http://dx.doi.org/10.1029/2009PA001850.

Stott, L., Poulsen, C., Lund, S., Thunell, R., 2002. Super ENSO and global climate oscillations at millennial time scales. Science 297, 222–226.

Tachikawa, K., Cartapanis, O., Vidal, L., Beaufort, L., Barlyaeva, T., Bard, E., 2011. The precession phase of hydrological variability in the Western Pacific Warm Pool during the past 400 ka. Quat. Sci. Rev. 30, 3716–3727.

Thompson, P.R., Be, A.W.H., Duplessy, J.C., Shackleton, N.J., 1979. Disappearance of pink-pigmented *Globigerinoides ruber* at 120,000 yr BP in the Indian and Pacific Oceans. Nature 280, 554–558.

Thunell, R., Tappa, E., Pride, C., Kincaid, E., 1999. Sea-surface temperature anomalies associated with the 1997–1998 El Niño recorded in the oxygen isotope composition of planktonic foraminifera. Geology 27, 843–846.

Toole, J.M., Millard, R.C., Wang, Z., Pu, S., 1990. Observations of the Pacific North Equatorial Current bifurcation at the Philippine coast. J. Phys. Oceanogr. 20, 307–318.

Trenberth, K.E., Caron, J.M., 2000. The Southern Oscillation revisited: sea level pressures, surface temperatures, and precipitation. J. Clim. 13, 4358–4365.

Tudhope, A.W., Chilcott, C.P., McCulloch, M.T., Cook, E.R., Chappell, J., Ellam, R.M., Lea, D.W., Lough, J.M., Shimmield, G.B., 2001. Variability in the El Niño-Southern oscillation through a glacial-interglacial cycle. Science 291, 1511–1517.

Waelbroeck, C., Labeyrie, L., Michel, E., Duplessy, J.C., McManus, J.F., Lambeck, K., Balbon, E., Labracherie, M., 2002. Sea-level and deep water temperature changes derived from benthic foraminifera isotopic records. Quat. Sci. Rev. 21, 295–305.

Xiang, R., Sun, Y., Li, T., Oppo, D.W., Chen, M., Zheng, F., 2007. Paleoenvironmental change in the middle Okinawa Trough since the last deglaciation: evidence from the sedimentation rate and planktonic foraminiferal record. Palaeogeogr. Palaeoclimatol. Palaeoecol. 243, 378–393.

Xiang, R., Chen, M., Li, Q., Liu, J., Zhang, L., Lu, J., 2009. Planktonic foraminiferal records of East Asia monsoon changes in the southern South China Sea during the last 40,000 years. Mar. Micropaleontol. 73, 1–13.

Yan, X.H., Ho, C.R., Zheng, Q., Klemas, V., 1992. Temperature and size variabilities of the Western pacific warm pool. Science 258, 1643–1645.

Yarincik, K.M., Murray, R.W., Peterson, L.C., 2000. Climatically sensitive eolian and hemipelagic deposition in the Cariaco Basin, Venezuela, over the past 578,000 years: results from Al/Ti and K/Al. Paleoceanography 15, 210–228.

Zhang, R., Delworth, T.L., 2005. Simulated tropical response to a substantial weakening of the Atlantic thermohaline circulation. J. Clim. 18, 1853–1860.

Zhang, Z., Leduc, G., Sachs, J.P., 2014. El Niño evolution during the Holocene revealed by a biomarker rain gauge in the Galápagos Islands. Earth Planet. Sci. Lett. 404, 420–434.

Zhang, S., Li, T., Chang, F., Yu, Z., Xiong, Z., Wang, H., 2016. Correspondence between the ENSO-like state and glacial-interglacial condition during the past 360 kyr. Chin. J. Oceanol. Limnol. 1–14. http://dx.doi.org/10.1007/s00343-017-6082-9.

Zheng, W., Braconnot, P., Guilyardi, E., Merkel, U., Yu, Y., 2008. ENSO at 6 ka and 21 ka from ocean-atmosphere coupled model simulations. Clim. Dyn. 30, 745–762.

Zhu, J., Liu, Z., Brady, E., Otto-Bliesner, B., Zhang, J., Noone, D., Tomas, R., Nusbaumer, J., Wong, T., Jahn, A., Tabor, C., 2017. Reduced ENSO variability at the LGM revealed by an isotope-enabled Earth system model. Geophys. Res. Lett. 44, 6984–6992.